A Dynamic Model for a Class of Semi-Autogenous Mill Systems

CHENG YUWEN[ID]**, BO SUN**[ID]**, AND SHUAI LIU**[ID]

School of Control Science and Engineering, Shandong University, Jinan 250061, China

Corresponding authors: Bo Sun (sunbo@sdu.edu.cn) and Shuai Liu (liushuai@sdu.edu.cn)

ABSTRACT In this paper, we develop a state space model of semi-autogenous (SAG) mill systems, which is of great significance to the mineral processing control. According to the practical enterprise production condition, the model is composed of two main parts. One is the ore circuit model. Compared with other models of ore circuit, the present model is simple and efficient. Another part is the SAG subsystem model where the state space model is utilized to depict the grinding mechanism. Furthermore, the grinding process of hold-ups are analyzed and presented with the common outputs such as power draw, pulp density and pulp flow. We consider the mass of rocks, granules and water as states and analyze the observability of the SAG subsystem model. For the ore circuit system and the SAG subsystem established respectively, unknown parameters of these models are identified by appropriate parameter estimation methods. Verified by the actual plant data, the result shows that the SAG mill system works well.

INDEX TERMS SAG mill system, dynamic model, parameter identification.

I. INTRODUCTION

With the development of mineral resources and the increasing demand for metals, the quantity of copper ore results in a relative request of preparation equipment. Because of the simple process, convenient configuration and low investment, the semi-autogenous (SAG) mill has been adopted increasingly in mines. The prominent feature of SAG mill is that copper rocks can be crushed by the strong impact on each other. As a rule, a little of water is added into the SAG mill to improve efficiency. Since the crushing process is a complex physical process which is related to the resistance strength, hardness, shape, size, humidity, density, particle size distribution and other factors, an applicable model of SAG system is hard to establish. The connections of variables and parameters has provided a remarkable challenge.

The solid system in the SAG mill cylinder is composed of a large number of discrete heterogeneous particles. The discrete element method (DEM) first proposed by Cundall has become a standard tool for processing such particulate matter. Mishra used DEM to analyse the trajectory of individual particles as well as contact force and the distribution

of energy [1]. The ball mill was further studied and DEM was adopted to predict the power [2]. Due to the large industrial equipment and complex distribution, DEM takes too much time to simulate the grinding process. In addition, the detailed granularity data is difficult to obtain. Therefore, it is particularly important to propose a macroscopic model analysis.

The dynamic model of SAG mill has attracted many researchers' attention. Apelt *et al.* made enormous contributions to the model and control for the SAG mill [3]–[6]. Considering the feed ore size distribution, Amestica *et al.* presented a dynamic model by taking the masses of water, copper rocks and granules as state variables [7], [8]. In [9], the control model was developed with taking the delivery rate of copper rocks, the feed flow rate of water and the rotation speed as control inputs and considering the power, the filling rate and particle size reduction as output variables. However, there is no sensor to measure the particle size in the SAG mill and the influence of rotation speed on the crushing rate is not considered. In [10], a class of SAG mill model was proposed in consideration of the influence of steel ball. Due to lacking of mining instrument and meter to measure the corresponding discharge, this method is not applicable. In [11], a relatively complete dynamic model was set up. The parameters need to be adjusted for different SAG

The associate editor coordinating the review of this manuscript and approving it for publication was Lei Jiao.

mill models. In power model and dynamic mathematical model, it was not taken into consideration that the volume of charge change with shoulder angle and toe angle in [12], [13]. When parameters need to be estimated, observability analysis of the model is necessary for the identification of the parameters. Whereas, in most of the existing literature, the observability was often neglected.

A variety of parameters in the SAG mill have been subjected to intensive studies. For example, the crushing rate is a crucial importance parameter in the operational process of SAG mill. According to the characteristics of ore, the total energy requirements of three common crushing machines were calculated in [14], which showed that the specific energy of SAG mill grinding is relatively high. The ore crushing model can be described by differential equations [11]. In the process of model simulation, errors accumulating with low accuracy was solved by matrix of differential equation of ore grinding in [15]. For the wet SAG mill, water was added into the cylindrical shell to drive out the copper granules smaller than the grid size. In [16], the retention of ore was expressed by linear fitting equation considering the parameters of grate open area, the location of apertures, mill speed and mill diameter. In [17], the influence of slurry discharge on power was analyzed, based which we know that slurry has little influence on power in the rolling mill. Latchireddi *et al.* studied the effect of grate's property, load and rotation speed on retention, then solved the complicated flow problem in rotating flow field by modeling the pulp hoist with fluid dynamics [18], [19]. In [20], time delay neural network was utilized to estimate particle sizes, which has a marked impact on fault diagnosis in the SAG grinding machine. In [21], the effect of mineral hardness on particle shape was analyzed by the detailed industrial data. The work index of characterizing the ore discharge rate affects the grade of copper ore, but the relation is difficult to be described by mathematical expression. In [22], the Rosin Rammler distribution was adopted to predict the dynamic function of particle size distribution in the SAG mill. In [23], the global sensitivity analysis is utilized to study the effect of the particle size distribution and the input variable on the working condition. By the analysis method, the particle size connection with other parameters was explored via data mining rather than mechanism analysis. As such, there are some difficulties to control the SAG subsystem by classical algorithms.

From the existing literature about dynamic model of the SAG mill system, the equipment in most studies included only the SAG mill but not the ore circuit. To the best of the authors' knowledge, this paper is the first study in the existing literature to consider the whole production line of copper ore pulp. Moreover, another contribution is confirming that the break rate of copper ore serves as a factor indirectly related to rotation speed of the SAG mill and the relationship is formulated. In this paper, considering the SAG mill system located in Inner Mongolia, we establish the mathematical model for the SAG mill system. First, we presents the grinding circuit and the model of ore feed system in Section II

and Section III. For the ore feeding system, a simple and effective model is given by the superposition of ore amount in the belt. We present the movement model of hold-ups within the SAG mill cylinder in Section IV. In Section V, based on mechanism analysis, special internal variables are selected to describe the measurement output for the SAG mill. In Section VI, the observability of SAG mill model is analyzed and unknown parameters are identified. Illustrative examples are presented in Section VII. Finally, we present the discussion and conclusion in Section VIII.

II. CIRCUIT DESCRIPTION

The grinding circuit to be considered consists of an ore bin, heavy-apron feeders, a SAG mill, vibrating screens and a pulp reservoir etc. This research is focused on the primary closed-loop grinding circuit as shown in Fig. 1.
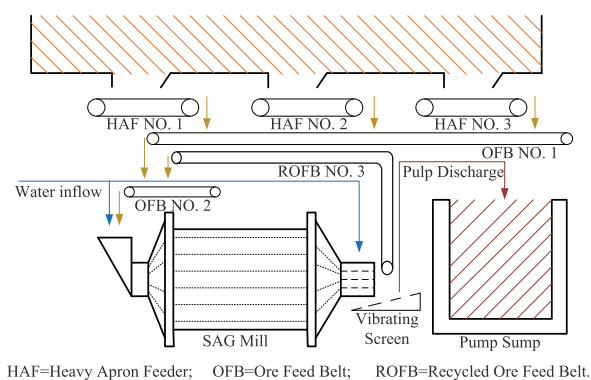

FIGURE 1. Process flow diagram of the SAG mill.

The fresh copper rocks are transported to the bin by trucks. There are three heavy-apron feeders under the ore bin, which are used to adjust the ore feeding rate by their motor frequencies. The operational mechanism is that the middle heavy-apron feeder is normally operated as a fine-tuned equipment and one of the heavy-apron feeders on the side is operated as the coarse adjustment. Ore bins above every heavy-apron feeder are installed with level indicators. Furthermore, the operating conditions of the three heavy-apron feeders are as follows

- The bilateral heavy-apron feeders are in operation alternatively.
- Each heavy-apron feeder is equipped with frequency detector to monitor the motor frequency.

According to the actual operation of the copper factory, the heavy-apron feeder NO. 1 and NO. 2 are working. The fresh ore is transferred to the ore feed belt NO. 1 from the heavy-apron feeder NO. 1 and NO. 2. Subsequently, the fresh ore is mixed with unqualified ore which is conveyed by the recycle ore feed belt NO. 3. The fresh copper ore and unqualified ore transferred from the ore feed belt NO. 1 and NO. 3 are sent into the SAG mill by the ore feed belt NO. 2. Ultimately, the pulp and unqualified ore are separated by the

vibrating screen. The liquidometer is installed on the pump sump.

All available measurements are as follows:
- Frequency of the heavy-apron feeder NO. 1 [Hz];
- Frequency of the heavy-apron feeder NO. 2 [Hz];
- Ore feed rate of the belt NO. 1 [t/h];
- Unqualified ore feed rate of the belt NO. 3 [t/h];
- Water inflow rate of the SAG mill [m^3/h];
- Discharging water flow rate [m^3/h];
- Discharging pulp flow rate [m^3/h];
- Power draw of the SAG mill [KW];
- Density of the discharged pulp [%].

III. ORE CIRCUIT MODEL

Since the copper rock is filled in the bin and piled up above the heavy plate, movement of the heavy-apron feeder plates drives the ore down. According to the structure feature of motor and electric machine theory, the speed of motor is proportional to the frequency. Taking delays into consideration, the relationship between the ore feed rate of the belt NO. 1 in the position of weighing transducer and motor frequencies of heavy-apron feeders can be given by

$$b_1(t) = a_1 f_1(t - \tau_1) + a_2 f_2(t - \tau_2), \quad (1)$$

where b_1 is the feed rate of fresh ore [t/s], f_1 is the motor frequency of the heavy-apron feeder NO. 1 [Hz], f_2 is the frequency of another heavy-apron feeder [Hz], τ_1 and τ_2 are time delays of the heavy-apron feeder NO. 1 and NO. 2, respectively [s], a_1 and a_2 are constants to be identified later.

In order to adjust the charge mass flow rate effectively in the actual production, frequencies of the ore feed belt NO. 1 and NO. 2 are normally fixed. In addition, the ore feed belt NO. 1 is distinct from the recycle ore feed belt NO. 3 in speed and belt width. Hence, the mass flow rate model of ore feed belt NO. 2 can be established in the similar way as follows

$$b_2(t) = a_3 b_1(t - \tau_3) + a_4 b_3(t - \tau_4), \quad (2)$$

where b_2 is the mass flow rate of belt NO. 2 in the location of the belt weighter [t/s], b_3 is the mass flow rate of the recycled ore feed belt NO. 3 [t/s], a_3 and a_4 are constants, τ_3 and τ_4 are time delays [s].

IV. SAG SUBSYSTEM MODEL

The internal mechanism model of SAG mill is established based on several commonly used observations. In particular, for the power model of SAG mill, we carry on the detailed analysis to the movement track of the internal material.

A. PULP DISCHARGE

Apelt *et al.* made a verification that the discharge flow rate with no pump sump is proportional to the square of the internal load [3]. For the SAG mill, the volume of pulp flow can be written as

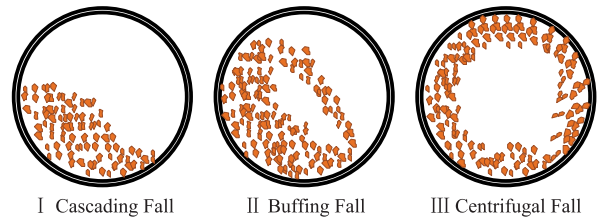$$Q = \eta \left(\frac{x_s}{\rho_s} + \frac{x_w}{\rho_w} \right)^2, \quad (3)$$

FIGURE 2. Three operational states.

I Cascading Fall   II Buffing Fall   III Centrifugal Fall

where x_s is the mass of the coper granules which can pass through the SAG mill discharge grate and always transform into the pulp mixing with water [t], x_w is the mass of water [t], Q is the output volume flow rate of pulp [m^3/s], η is a constant, ρ_s is the average density of copper rocks [t/m^3], ρ_w is the water density [t/m^3].

B. DENSITY

Pulp density is an important physical quantity which reflects grinding characteristics of the copper mine. The concentration of discharge pulp is given by

$$C = \frac{x_s}{x_w + x_s}, \quad (4)$$

where C is the discharge pulp density [%].

C. POWER DRAW

The power draw P [KW] includes not only the idle power P_0 [KW] but also the load power P_1 [KW] which is mainly affected by the load and the rotation speed of the SAG mill cylinder shell. Hence, the power can be represented by

$$P = P_0 + P_1. \quad (5)$$

The SAG mill is operated under three conditions theoretically like Fig. 2. Whereas, it is always operated in the second fall mode in practical production. The cross section of the cylinder shows that each layer movement of hold-ups consists of the ore rocks, granules and water as shown in Fig. 3. For the SAG mill model, there are some assumptions as follows

- The hold-ups will not drift to other grinding layers during the movement.
- Speeds of the hold-ups are reduced to zero at point B shown in Fig. 3.
- The rotational speed remains the same in a rotational period.
- The energy consumption caused by friction is negligible.

Apparently, when the radius equals to r shown in Fig. 3, the maximal drop height H^r is given by

$$H^r = Y_B^r + h^r, \quad (6)$$

where Y_B^r is the falling height from point A to point B [m], h^r is the lift height [m].

Combining with the force analysis of hold-ups at point A when the radius equals to r, the expression of centripetal force
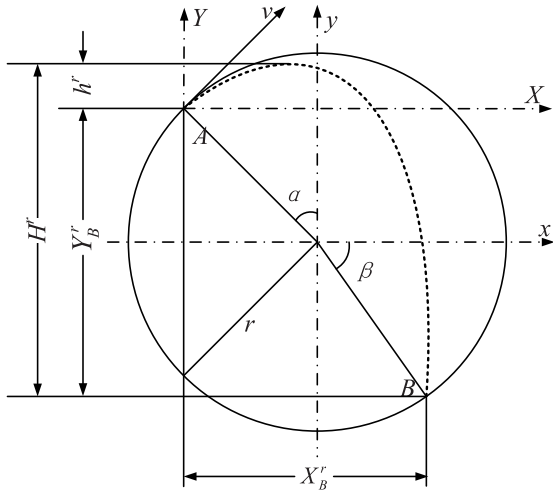
FIGURE 3. Motion curves of hold-ups in the SAG mill.

is expressed as

$$mg \cos \alpha = mr\omega^2 = m\frac{v^2}{r}, \tag{7}$$

where m is the mass of the hold-ups at point A $[t]$, g is the gravitational acceleration $[m/s^2]$, α is the shoulder angle $[rad]$, ω is the angular velocity of the hold-ups $[rad/s]$, v is the tangential velocity $[m/s]$.

By simplifying (7), the relationship between the shoulder angle and the tangential velocity of the hold-ups is obtained by

$$v^2 = gr \cos \alpha. \tag{8}$$

Substituting the common formula of circular motion $v = \frac{\pi r n}{30}$ into (8), the relation between the radical position and the charge shoulder angle is given by

$$r = \frac{900g}{n^2\pi^2} \cos \alpha, \tag{9}$$

where n is the rotation speed $[r/min]$. When the rotational speed is fixed, the shoulder angle depends on the radical position of charge inner surface radius of mill inside liners.

The movement locus of hold-ups is analyzed in rectangular coordinates after the the hold-ups leaving point A shown in Fig. 3. Building the two-dimensional reference frame with the origin at point A, we can get trajectory equations of the parabola and the circle such that

$$y = x \tan \alpha - \frac{gx^2}{2v^2\cos^2\alpha}, \tag{10a}$$

$$(x - r \sin \alpha)^2 + (y + r \cos \alpha)^2 = r^2, \tag{10b}$$

where x and y are the horizontal and vertical coordinates.

From the simultaneous equations (10a) and (10b), the set of coordinate values at point B is given by

$$X_B^r = 4r \sin \alpha \cos^2\alpha, \tag{11a}$$

$$Y_B^r = 4r\sin^2\alpha \cos \alpha, \tag{11b}$$

where X_B^r is the horizontal coordinate, Y_B^r is the vertical coordinate.

Applying Newton's Second Law, the lift height with the radial distance equal to r can be governed by

$$h^r = \frac{v^2\sin^2\alpha}{2g}. \tag{12}$$

Substituting (11b) and (12) into (6), we obtain the maximum of falling height when the radius equals to r as follows

$$\begin{aligned} H^r &= \frac{v^2\sin^2\alpha}{2g} + 4r\sin^2\alpha \cos \alpha \\ &= \frac{gr\cos^2\alpha\sin^2\alpha}{2g} + 4r\sin^2\alpha \cos \alpha \\ &= 4.5r\sin^2\alpha \cos \alpha. \end{aligned} \tag{13}$$

Moreover, we can get

$$\tilde{X}_B^r = X_B^r - r \sin \alpha = 4r \sin \alpha \cos^2\alpha - r \sin \alpha. \tag{14}$$

Therefore the numerical calculation of the minimum radial position of charge inner surface is gained by $\frac{dX_B^r}{dt} = 0$. By simple manipulation, the result is given by

$$16\cos^4\alpha - 14\cos^2\alpha + 1 = 0. \tag{15}$$

By solving (15) and substituting the result into (9), the minimum radius can be expressed as

$$R_{min} = \frac{252.10}{n^2}, $$

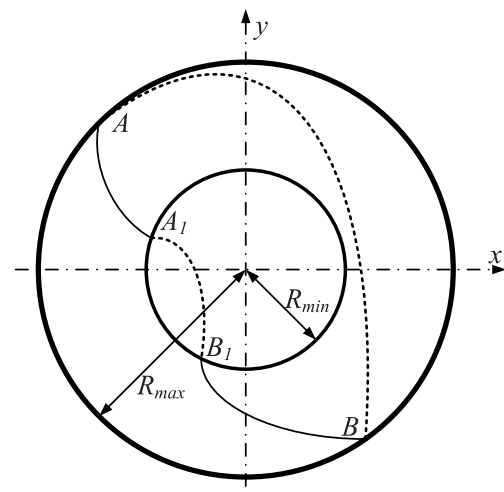where R_{min} is the minimum radical position.

FIGURE 4. Maximum radius and minimum radius.

From the view of cross section shown in Fig. 4, when one of the layers is under the optimum condition, the others may not be under the optimum conditions. Hence, the polycondensation layer is introduced to concentrate masses of all layers

to one layer. The radius R of the polycondensation layer is given by

$$R = \sqrt{\frac{R_{max}^2 + R_{min}^2}{2}}, \tag{16}$$

where R_{max} is the maximum radius [m].

The maximum falling height of the polycondensation layer is expressed as

$$H = 4.5R\sin^2\alpha \cos\alpha. \tag{17}$$

Since different layers have different rotational periods, we utilize the period of the ploycondensation layer to represent whole. The rotational period t_0^R is the time that it takes to revolve when the radius equals to R in (16). The SAG mill drives the hold-ups to revolve during the rotational period. Hence, the loading power is expressed as

$$P_1 = \frac{E}{t_0^R} \tag{18}$$

where E is the energy provided the hold-ups to revolve by the SAG motor [KJ], t_0^R is the rotational period [s].

When the cylinder rotates, the impact energy E of the hold-ups for a certain paraboloid is given by

$$dE = \frac{1}{2}v_B^2 dm, \tag{19}$$

where v_B is the velocity at point B [m/s], dm is the differential form of the layer mass [t] which can be described by

$$dm = \sigma \omega r t_2 dr, \tag{20}$$

where σ is the line mass [t/m^2], ω is the angular speed of the barrel [rad/s], t_2 is the movement time in circular when the radius equals to r [s].
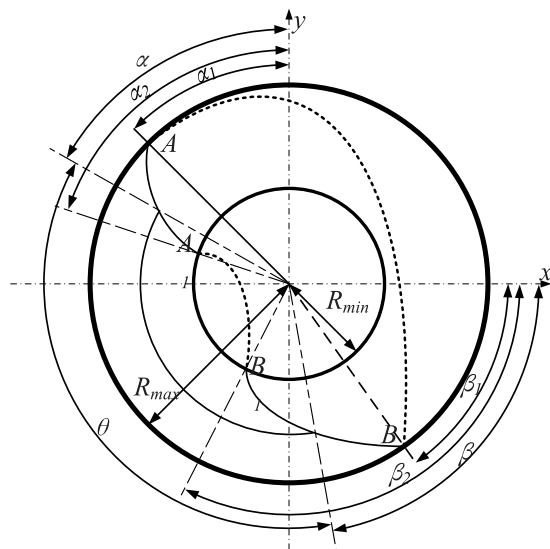

FIGURE 5. Area of hold-ups in the SAG mill.

The total mass of mixture is related to the two time periods. One is the movement time in a cycle period t_1 and the other is the duration time in the paraboloid t_2. As shown in Fig. 5,

because t_1 and t_2 are the movement time periods when the radius equals to r, we utilize the time in every layer to express the whole time period which is closely related to the mass in the circular surface and paraboloid. We utilize a ratio to represent the relationship as below

$$M_1 = \frac{\int_{R_{min}}^{R_{max}} t_1 dr}{\int_{R_{min}}^{R_{max}} (t_1 + t_2)dr}M, \tag{21}$$

where M_1 is the total mass in the circular surface [t], t_1 is the movement time period in the paraboloid [s]. M is the total mass of hold-ups in the cylinder of the SAG mill [t], i.e.

$$M = x_r + x_w + x_s,$$

where x_r is mass of copper rocks in the SAG mill [t].

The coordinate of B (11b) is substituted into the trigonometric function of β. The relationship between the shoulder angle and toe angle is given by

$$\begin{aligned}
\sin\beta &= \frac{Y_B^r - r\cos\alpha}{r} \\
&= \frac{4r\sin^2\alpha\cos\alpha - r\cos\alpha}{r} \\
&= 3\cos\alpha - 4\cos^3\alpha. \tag{22}
\end{aligned}$$

By simplifying (22), the following relationship is obtained

$$\beta = 3\alpha - \frac{\pi}{2}.$$

By the assumption that the rotational speed remains the same in a rotational period, we can obtain the duration when the particle moves along the circle as follows

$$t_1 = \frac{2\pi - 4\alpha}{2\pi} \Big/ \frac{n}{60} = \frac{60(\pi - 2\alpha)}{n\pi}.$$

Substituting the coordinate (11a) into simple kinematics formulas, the paraboloid time is shown as

$$t_2 = \frac{X_B^r}{v\cos\alpha} = \frac{60\sin 2\alpha}{n\pi}. \tag{23}$$

The total time in a rotational period can be given by

$$t_0 = \frac{60(\pi + \sin 2\alpha - 2\alpha)}{\pi n}. \tag{24}$$

When the radius r equals to R in (9), the shoulder angle is rewritten as

$$\alpha = \arccos\frac{Rn^2\pi^2}{900g}.$$

Substituting this equation into (24), t_0^R is obtained by

$$t_0^R = \frac{60}{n} + \frac{2nR\pi\sqrt{1 - \frac{R^2n^4\pi^4}{30^4g^2}}}{15g} - \frac{120\arccos\left(\frac{Rn^2\pi^2}{30^2g}\right)}{\pi n}. \tag{25}$$

Substituting (23) and (24) into (21), we can obtain

$$M_1 = \frac{M\left[(6\alpha - 3\pi)\cos\alpha - 6\sin\alpha\right]\big|_{\alpha_2}^{\alpha_1}}{\left[(6\alpha - 3\pi)\cos\alpha + 2\sin^3\alpha - 6\sin\alpha\right]\big|_{\alpha_2}^{\alpha_1}}. \tag{26}$$

In the circular surface, the line mass is the ratio of the total mass of hold-ups to the area which is given by

$$\sigma = \frac{M_1}{S_1}, \tag{27}$$

where S_1 is the area of mixture in the circular surface $[m^2]$.

The differential area of the charge in the parabolic surface is shown as follows

$$
\begin{aligned}
dS_1 &= r\theta dr \\
&= -\frac{30^4 g^2}{\pi^4 n^4}\left(\frac{3}{2}\pi - \alpha - \beta\right)\cos\alpha\sin\alpha d\alpha \\
&= -\frac{30^4 g^2}{\pi^4 n^4}(\pi - 2\alpha)\sin 2\alpha d\alpha.
\end{aligned}
$$

The analytical form of S_1 is given by

$$S_1 = \frac{30^4 g^2}{\pi^4 n^4}\left[\frac{(\pi-2\alpha)\cos 2\alpha + \sin 2\alpha}{2}\right]\Big|_{\alpha_2}^{\alpha_1}. \tag{28}$$

Substituting (28) and (26) into (27), we get

$$\sigma = \beta(x_s + x_r + x_w), \tag{29}$$

where

$$\beta = \frac{2n^4\pi^4}{30^4 g^2\left[(6\alpha-3\pi)\cos\alpha + 2\sin^3\alpha - 6\sin\alpha\right]\Big|_{\alpha_2}^{\alpha_1}} \times \frac{[(6\alpha-3\pi)\cos\alpha - 6\sin\alpha]\Big|_{\alpha_2}^{\alpha_1}}{[(\pi-2\alpha)\cos 2\alpha - \sin 2\alpha]\Big|_{\alpha_2}^{\alpha_1}}.$$

By simple transformations and substitutions of (7) and (13), v_B is obtained by

$$
\begin{aligned}
v_B &= \sqrt{(v\cos\alpha)^2 + 2gH^r} \\
&= v\sqrt{9 - 8\cos^2\alpha}.
\end{aligned}
\tag{30}
$$

Substituting (20) and (30) into (19), we get the differential form of the energy such that

$$dE = \frac{1}{2}\sigma\omega r t_2 v^2\left(9 - 8\cos^2\alpha\right)dr, \tag{31}$$

where $\omega = \frac{2\pi n}{60}$.

Substituting (8), (9) and (23) into (31), the following compact form is obtained as follows

$$dE = -\frac{30^6 g^4\sigma}{\pi^6 n^6}\cos^3\alpha\left(9 - 8\cos^2\alpha\right)\sin 2\alpha\sin\alpha d\alpha. \tag{32}$$

Integrating (32) from α_1 to α_2 yields that

$$
\begin{aligned}
&= -\frac{30^6 g^4\sigma}{\pi^6 n^6} \\
&\quad \times \frac{\left(12\cos^7\alpha - 20\cos^5\alpha + 2\cos^3\alpha + 3\cos\alpha\right)\sin\alpha + 3\alpha}{24}\Big|_{\alpha_2}^{\alpha_1}.
\end{aligned}
\tag{33}
$$

In (26) and (33), α_2 is the solution to equation (15). When the radius equals to R_{max} in (9), we can obtain

$$\alpha_1 = \arccos\frac{\pi^2 n^2 R_{max}}{900 g}.$$

Substituting (33), (29) and (25) into (18), we can obtain the loading power P_1 such that

$$P_1 = \lambda(x_s + x_r + x_w),$$

with

$$
\begin{aligned}
\lambda = &-\frac{30^6\ g^4\beta}{n^6\pi^6} \\
&\times \frac{\left(12\cos^7\alpha - 20\cos^5\alpha + 2\cos^3\alpha + 3\cos\alpha\right)\sin\alpha + 3\alpha}{24\ t_0^R}\Big|_{\alpha_2}^{\alpha_1}.
\end{aligned}
$$

Ultimately, the power draw can be written as

$$P = P_0 + \lambda(x_s + x_r + x_w), \tag{34}$$

where λ is a time-varying parameter. Due the computational process is readily comprehensible but too rigmarole, we can facilely solve with the MATLAB program.

V. DYNAMIC MODEL
A. DYNAMIC MODEL OF SAG MILL
In this subsection, we consider the case that the coper ore is classified into two types: the rocks and granules. The granules rather than the rocks can pass through the discharge grate of SAG mill. In this case, we can separate them individually. Thus, the masses of rocks, granules and water in the cylindrical shell will be considered as states.

1) COPPER ROCKS
Copper ore is ground by collision with itself and the wear-resistant lining. The mass of copper rocks in the SAG mill cylinder x_r can be described as a first-order system as follows

$$\frac{dx_r}{dt} = u_r - K_r x_r - q_n, \tag{35}$$

where u_r is the feed rate of copper rocks $[t/s]$, K_r is the crushing rate of copper rocks $[s^{-1}]$, q_n is the unqualified ore $[t/s]$.

The crushing rate of copper rocks K_r is affected by the maximum of falling height in the ploycondensation layer H. In (9), the shoulder angle depends on the rotation speed when the radius equals to r. In (17), the maximum value of H can be gained by $\frac{dH}{d\alpha} = 0$ such that

$$\frac{dH}{d\alpha} = \frac{d\left(4.5R\sin^2\alpha\cos\alpha\right)}{d\alpha} = 0.$$

When H reaches the maximum H_{max}, $\alpha = 0.304\pi$. Substituting (9) into (17), the relationship between the maximum of falling height in the ploycondensation layer H and the rotate n can be given as

$$H(n) = \frac{4.5\pi^2 n^2 R^2\left(30^4 g^2 - \pi^4 n^4 R^2\right)}{30^6 g^3}. \tag{36}$$

Hence,

$$K_r = \gamma \bar{K}_r, \qquad (37)$$

where $\bar{K}_r$ is the maximal crushing rate of copper ore, γ is a time-varying coefficient which is denoted by

$$\gamma = \frac{H(n)}{H_{max}}.$$

2) GRANULES

The granule is the solid particle which can pass through the discharge grate of SAG mill. The granule formed of the ground copper rocks is blended with the water, and eventually forms the pulp. Hence, the change of granules can be expressed as

$$\frac{dx_s}{dt} = -c_s + K_r x_r, \qquad (38)$$

where c_s is the discharge rate of granules $[t/s]$.

3) WATER

The content of water varies with input and output flow rates. The dynamic model of water is given by

$$\frac{dx_w}{dt} = -c_w + u_w, \qquad (39)$$

where u_w is the input rate of water $[t/s]$, c_w is the water discharge rate accompanying with the pulp $[t/s]$.

The outflow rates of water and granules are described in detail [10]. They can be shown as

$$c_s = \eta(x_w + x_s)x_s,$$
$$c_w = \eta(x_w + x_s)x_w.$$

B. STATE SPACE EXPRESSION

The state space model is used to describe dynamic changes of internal states including the mass of water, copper rocks and granules in the SAG mill. Denote

$$x = \begin{bmatrix} x_r & x_s & x_w \end{bmatrix}^T.$$

Combining (35), (38) and (39), the state space model can be expressed as

$$\begin{bmatrix} \dot{x}_s \\ \dot{x}_r \\ \dot{x}_w \end{bmatrix} = \begin{bmatrix} -\eta(x_w + x_s)x_s + K_r x_r \\ -K_r x_r - q_n \\ -\eta(x_w + x_s)x_w \end{bmatrix} + \begin{bmatrix} 0 \\ u_r \\ u_w \end{bmatrix}. \qquad (40)$$

By integrating (3), (4) and (34), the output equation is expressed as

$$\begin{bmatrix} P \\ Q \\ C \end{bmatrix} = \begin{bmatrix} P_0 + \lambda(x_r + x_w + x_s) \\ \eta\left(\dfrac{x_s}{\rho_s} + \dfrac{x_w}{\rho_w}\right)^2 x_s \\ \dfrac{x_s}{x_s + x_w} \end{bmatrix}. \qquad (41)$$

VI. PARAMETER IDENTIFICATION

A. ORE FEEDING SYSTEM

Recursive least-square method is used to identify the parameters a_1, a_2, a_3 and a_4. Combining (1) and (2), we obtain that

$$\begin{bmatrix} b_1(k) \\ b_2(k) \end{bmatrix} = \begin{bmatrix} a_1 & a_2 & 0 & 0 \\ 0 & 0 & a_3 & a_4 \end{bmatrix} \begin{bmatrix} f_1(k - \tau_1) \\ f_2(k - \tau_2) \\ b_1(k - \tau_3) \\ b_3(k - \tau_4) \end{bmatrix}. \qquad (42)$$

Denote

$$z(k) = \begin{bmatrix} b_1(k) & b_2(k) \end{bmatrix}^T,$$
$$\theta = \begin{bmatrix} a_1 & a_2 & a_3 & a_4 \end{bmatrix}^T,$$
$$\Gamma(k) = \begin{bmatrix} f_1(k - \tau_1) & 0 \\ f_2(k - \tau_2) & 0 \\ 0 & b_1(k - \tau_3) \\ 0 & b_3(k - \tau_4) \end{bmatrix}.$$

The ore feeding system (42) is described in the following compact form

$$z(k) = \Gamma^T(k)\theta.$$

The criterion function is chosen as

$$J(\theta) = \sum_{k=1}^{L} \left\| z(k) - \Gamma^T(k)\theta \right\|_2. \qquad (43)$$

According to the principle of least square method, the recursive formula of the parameter estimation of the multiple input multiple output system is given by

$$\begin{cases} \theta(k) = \theta(k - 1) + K(k)[y(k) - \Gamma^T(k)\theta(k - 1)] \\ K(k) = L(k - 1)\Gamma(k)[I_m + \Gamma^T(k)L(k - 1)\Gamma(k)]^{-1} \\ L(k) = [I - K(k)\Gamma^T(k)]L(k - 1), \end{cases} \qquad (44)$$

where K is the gain of correction, L is the recursive factor and I is the identity matrix.

B. SAG SUBSYSTEM

Since the values of ρ_s and ρ_w are gained by the experimental measurement, parameters $\bar{K}_r$ and η in the dynamic model can be identified by extend Kalman filter. By discretizing (40) and (41), the discrete system model is obtained by

$$\begin{bmatrix} x_s(k+1) \\ x_r(k+1) \\ x_w(k+1) \end{bmatrix} = \begin{bmatrix} x_s(k) - \eta x_{ps}(k) + K_r(k)x_r(k) \\ x_r(k) - K_r(k)x_r(k) - q_n(k) \\ x_w(k) - \eta x_{pw}(k) \end{bmatrix} + \begin{bmatrix} 0 \\ u_r(k) \\ u_w(k) \end{bmatrix}, \qquad (45)$$

and

$$\begin{bmatrix} P(k) \\ Q(k) \\ C(k) \end{bmatrix} = \begin{bmatrix} P_0 + \lambda(k)\left(x_r(k) + x_p(k)\right) \\ \eta\left(\dfrac{x_s(k)}{\rho_s} + \dfrac{x_w(k)}{\rho_w}\right)^2 \\ \dfrac{x_s(k)}{x_p(k)} \end{bmatrix}, \qquad (46)$$

where $x_{ps}(k) = [x_w(k) + x_s(k)]x_s(k)$, $x_{pw}(k) = [x_w(k) + x_s(k)]x_w(k)$ and $x_p(k) = x_w(k) + x_s(k)$.

Observability represents the ability that the system state can be fully reflected by the output. In order to estimate parameters in (45) and (46), we incorporate $\bar{K}_r$ and η into the state and obtain the following augmented system. Denote

$$X_k = \begin{bmatrix} x_s(k) & x_r(k) & x_w(k) & \bar{K}_r & \eta \end{bmatrix}^T. \quad (47)$$

After system augmentation, the system matrix is rewritten as

$$f(X_k) = \begin{bmatrix} x_s(k) - \eta x_{ps}(k) + \gamma(k)\bar{K}_r x_r(k) \\ x_r(k) - \gamma(k)\bar{K}_r x_r(k) - q_n(k) \\ x_w(k) - \eta x_{pw}(k) \\ \bar{K}_r \\ \eta \end{bmatrix}.$$

Similarly, the output matrix can be given by

$$h(X_k) = \begin{bmatrix} \lambda(k)\left(x_r(k) + x_p(k)\right) \\ \eta\left(\dfrac{x_s(k)}{\rho_s} + \dfrac{x_w(k)}{\rho_w}\right) \\ \dfrac{x_s(k)}{x_p(k)} \end{bmatrix}.$$

Taylor expansion of the nonlinear function at $\hat{X}_k$ is given by

$$f(X_k) = f(\hat{X}_k) + \tilde{F}_k(X_k - \hat{X}_k),$$
$$h(X_k) = h(\hat{X}_k) + \tilde{H}_k(X_k - \hat{X}_k),$$

where $\tilde{F}_k$ and $\tilde{H}_k$ are the Jacobian matrix to linearize the system at the operation point calculated by

$$\begin{cases} \tilde{F}_k = \left.\dfrac{\partial f(X_k)}{\partial x}\right|_{X=\hat{X}_k} \\ \tilde{H}_k = \left.\dfrac{\partial h(X_k)}{\partial X}\right|_{X=\hat{X}_k}. \end{cases}$$

It is easy to verify that the linearized system is completely observable. The system matrix and output matrix after discretization are given by

$$\tilde{F}_k = \begin{bmatrix} \tilde{F}_{11}(k) & \gamma(k)\bar{K}_r & -\eta x_s(k) & \gamma(k)x_r(k) & -x_{ps}(k) \\ 0 & 1-\gamma(k)\bar{K}_r & 0 & -\gamma(k)x_r(k) & 0 \\ -\eta x_w(k) & 0 & \tilde{F}_{33}(k) & 0 & -x_{pw}(k) \\ 0 & 0 & 0 & 1 & 0 \\ 0 & 0 & 0 & 0 & 1 \end{bmatrix},$$

and

$$\tilde{H}_k = \begin{bmatrix} \lambda(k) & \lambda(k) & \lambda(k) & 0 & 0 \\ \dfrac{\eta}{\rho_s} & 0 & \dfrac{\eta}{\rho_w} & 0 & \dfrac{x_s(k)}{\rho_s} + \dfrac{x_w(k)}{\rho_w} \\ \dfrac{x_w(k)}{x_p^2(k)} & 0 & -\dfrac{x_w(k)}{x_p^2(k)} & 0 & 0 \end{bmatrix},$$

where $\tilde{F}_{11}(k) = 1 - \eta[2x_s(k) + x_w(k)]$ and $\tilde{F}_{33}(k) = 1 - \eta[2x_w(k) + x_s(k)]$.

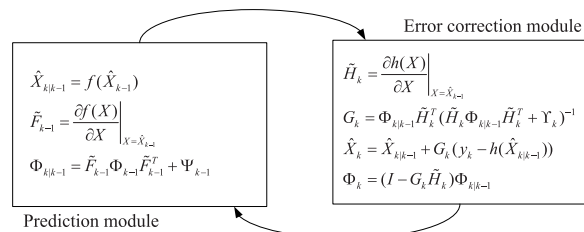The validation has been done by the SAG mill at Inner Mongolia Huogeqi copper mine. Discrete nonlinear system

FIGURE 6. Extended Kalman filter algorithm.

TABLE 1. Basic parameter value.

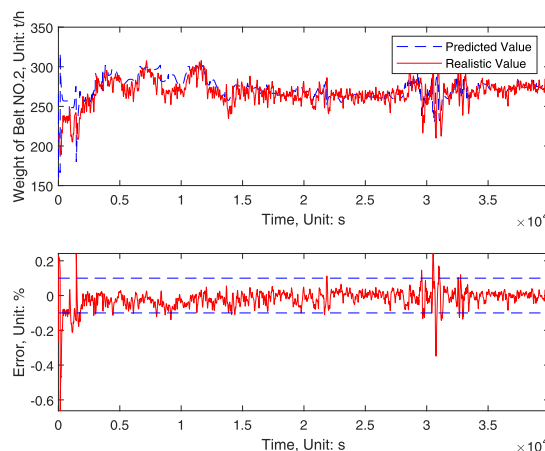| Parameter	Value	Unit
τ_1	40	s
τ_2	40	s
τ_3	110	s
τ_4	120	s
g	9.8	m/s^2
R_{max}	4	m

FIGURE 7. Fresh copper ore regulated by heavy-apron feeders.
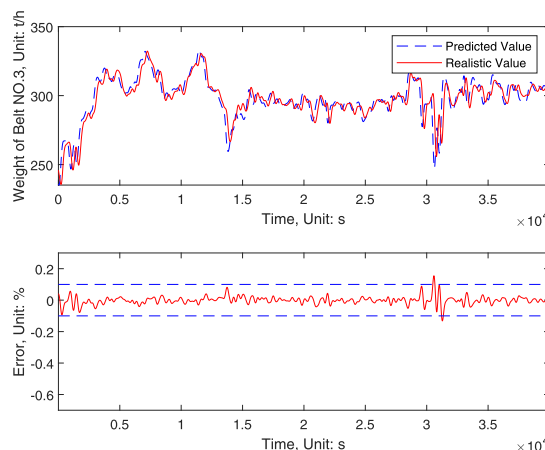

FIGURE 8. Copper ore of the SAG mill charge.

equations are approximated as linear functions by the polynomial expansion method as follows

$$\begin{cases} X_{k+1} = f(\hat{X}_k) + \tilde{F}_k(X_k - \hat{X}_k) + u(k) \\ y_k = h(\hat{X}_{k|k-1}) + \tilde{H}_k(X_k - \hat{X}_{k|k-1}), \end{cases} \quad (48)$$
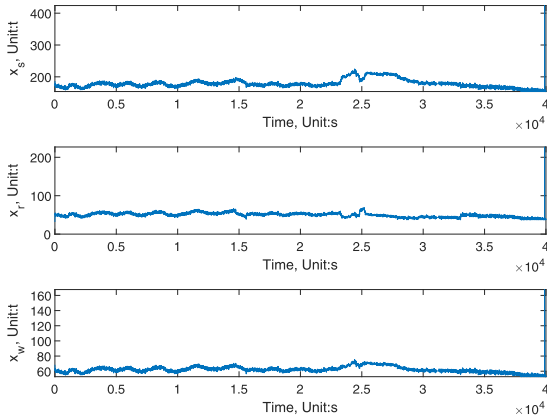
FIGURE 9. Four estimated states of the SAG mill.

FIGURE 10. Power draw of the SAG mill in the prediction.
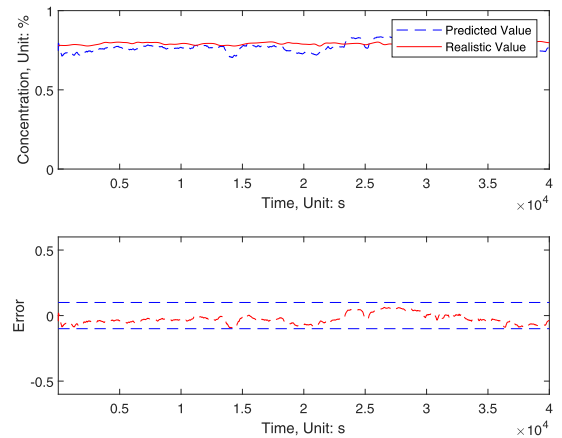
FIGURE 11. Concentration of pulp in the prediction.

FIGURE 12. Pulp flow in the prediction.

where $u(k) = \begin{bmatrix} 0 & u_r(k) & u_w(k) & 0 & 0 \end{bmatrix}^T$ and $y(k) = \begin{bmatrix} P(k) & Q(k) & C(k) \end{bmatrix}^T$. By applying observability criterion to linearized system (48), we find that the states are observable in the system (48). We then adopt extended Kalman filter to estimate parameters which is a recursive algorithm based on prior estimations and posterior estimations. It is composed of prediction module and error correction module as shown in Fig. 6.

VII. SIMULATION

With the real data collected from the mine, we identify parameters to ensure the model practicability.

A. ORE FEED SIMULATION

Before the parameter identification, some basic data provided by operators are given in Table 1. In addition, the delays in the ore belt system model (1) and (2) are averaged by multiple measurements.

The estimation parameter θ minimizes the criterion function (43) with the optimal value given by

$$\theta = \begin{bmatrix} a_1 \\ a_2 \\ a_3 \\ a_4 \end{bmatrix} = \begin{bmatrix} 9.151 \\ 8.743 \\ 1.417 \\ 0.961 \end{bmatrix}.$$

B. SAG MILL SIMULATION

Before estimating parameters by extended Kalman filter method, we used the real data to illustrate the correctness of the SAG mill model.

The initialisation of the observer is given by Table 2. By iteration operation, estimated values of parameters in the SAG mill model are given by

$$\begin{cases} K_r = 0.8191 \\ \eta = 0.00012. \end{cases} \tag{49}$$

In the standard dynamic system of the SAG mill, state variables of mill are masses of copper rocks x_r, granules x_s and water x_w which are described in Fig. 9.
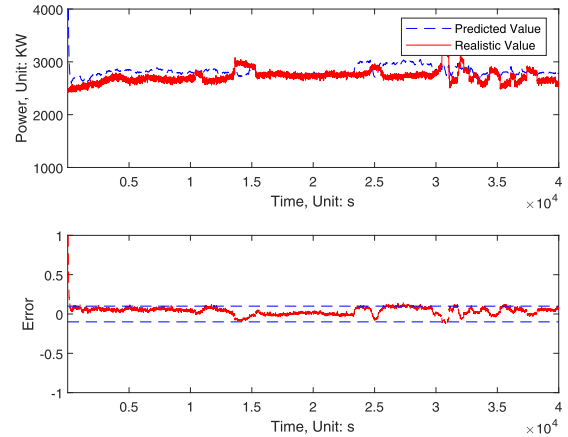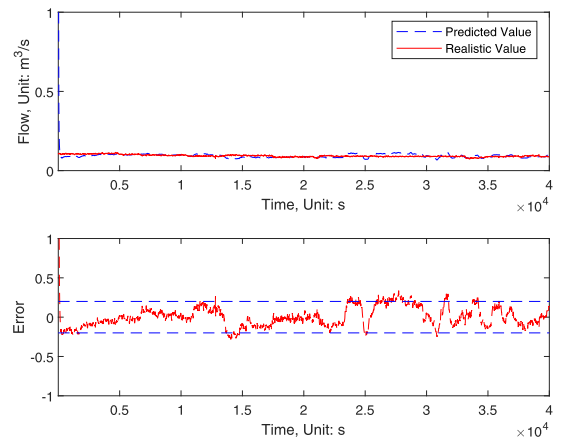
Utilizing the estimated parameters, we continue to simulate with another set of data to predict system outputs. The sample interval T is $1s$. Based on obtained results shown in Fig. 10, it can be confirmed that the predicted power P and real production data match well.

Description	Initialisation value
State of initial values	$X_0 = \begin{bmatrix} 70 & 40 & 33 & 0.05 & 0.001 \end{bmatrix}^T$
Covariance matrix of the noise process	$\Psi_k = diag \begin{bmatrix} 0.5 & 0.4 & 0.3 & 5 \times 10^{-3} & 1 \times 10^{-5} \end{bmatrix}$
Covariance matrix of the output noise	$\Upsilon_k = diag \begin{bmatrix} 10 & 0.01 & 0.05 \end{bmatrix}$
Initial error covariance matrix	$\Phi_0 = I_{5 \times 5}$

As is seen from the result obtained by parameters estimation, the model can adapt to the influence of the change of control input from the perspective of qualitative and quantitative analysis.

VIII. CONCLUSION

In this paper, we proposed a complete model for the SAG mill systems including ore feeding system and SAG subsystem. The ore feeding quantity is usually controlled by adjusting the frequencies of asynchronous motors in the the heavy-apron feeder system. The feeding model proposed in this paper has a strong migration adaptability and can meet the control requirement for the engineering designer. In the paper, a standard dynamic model is established for a class of SAG mill from the perspective of mechanism analysis. The content of copper rocks, granules and water are taken as state variables, which conforms to the practical application system. For the SAG subsystem, we introduced our pioneer work on establishing the relationship between the hold-ups and power. In addition, internal states of the SAG mill system are described in detail. The average falling height and other important time-varying parameters are derived by means of the rotational speed. In this way, the relations between states and outputs in the SAG subsystem can be described, so as to reduce complexity of the model as well as the number of estimated parameters and to improve migration adaptability of the model.

The ore feed control system and the SAG subsystem constitute a complete mine grinding process model which has instructive significance in the whole ore dressing operation. In the SAG subsystem, according to the ore particle size, the copper ore is divided into two categories. One is the granule which can pass through the discharge grate. Another is the copper rock which cannot pass through and is crushed in the cylindrical shell. The classified method is cursory. However, there is no sensor to measure the distribution of particle size when the copper ore is crushing in the SAG mill. From mining to slurry outflow, the whole process industry control design is inseparable from a complete model. Thus, the following work is to apply the optimization algorithm and design the controller based on this model.

REFERENCES

[1] B. K. Mishra, "A review of computer simulation of tumbling mills by the discrete element method: Part I—Contact mechanics," *Int. J. Mineral Process.*, vol. 71, nos. 1–4, pp. 73–93, Sep. 2003.

[2] B. K. Mishra, "A review of computer simulation of tumbling mills by the discrete element method: Part II—Practical applications," *Int. J. Mineral Process.*, vol. 71, no. 1, pp. 95–112, 2003.

[3] T. A. Apelt, S. P. Asprey, and N. F. Thornhill, "Inferential measurement of SAG mill parameters," *Minerals Eng.*, vol. 14, no. 6, pp. 575–591, Jun. 2001.

[4] T. A. Apelt, S. P. Asprey, and N. F. Thornhill, "Inferential measurement of SAG mill parameters II: State estimation," *Minerals Eng.*, vol. 15, no. 12, pp. 1043–1053, Dec. 2002.

[5] T. A. Apelt, S. P. Asprey, and N. F. Thornhill, "Inferential measurement of SAG mill parameters III: Inferential models," *Minerals Eng.*, vol. 15, no. 12, pp. 1055–1071, 2002.

[6] T. A. Apelt and N. F. Thornhill, "Inferential measurement of SAG mill parameters IV: Inferential model validation," *Minerals Eng.*, vol. 22, no. 12, pp. 1032–1044, Oct. 2009.

[7] R. Amestica, G. D. Gonzalez, J. Menacho, and J. Barria, "A mechanistic state equation model for semiautogenous mills," *Int. J. Mineral Process.*, vols. 44–45, pp. 349–360, Mar. 1996.

[8] T. A. Apelt and N. F. Thornhill, "Inferential measurement of SAG mill parameters V: MPC simulation," *Minerals Eng.*, vol. 22, no. 12, pp. 1045–1052, Oct. 2009.

[9] J.-L. Salazar, H. Valdés-González, E. Vyhmeister, and F. Cubillos, "Model predictive control of semiautogenous mills (SAG)," *Minerals Eng.*, vol. 64, pp. 92–96, Oct. 2014.

[10] J. D. le Roux, A. Steinboeck, A. Kugi, and I. K. Craig, "An EKF observer to estimate semi-autogenous grinding mill hold-ups," *J. Process Control*, vol. 51, pp. 27–41, Mar. 2017.

[11] J. L. Salazar, L. Magne, G. Acuña, and F. Cubillos, "Dynamic modelling and simulation of semi-autogenous mills," *Minerals Eng.*, vol. 22, no. 1, pp. 70–77, Jan. 2009.

[12] W. Valery and S. Morrell, "The development of a dynamic model for autogenous and semi-autogenous grinding," *Minerals Eng.*, vol. 8, no. 11, pp. 1285–1297, Nov. 1995.

[13] S. Morrell, "A new autogenous and semi-autogenous mill model for scale-up, design and optimisation," *Minerals Eng.*, vol. 17, no. 3, pp. 437–445, Mar. 2004.

[14] S. Morrell, "Predicting the overall specific energy requirement of crushing, high pressure grinding roll and tumbling mill circuits," *Minerals Eng.*, vol. 22, no. 6, pp. 544–549, May 2009.

[15] P. Yu, W. Xie, L. X. Liu, and M. S. Powell, "Analytical solution for the dynamic model of tumbling mills," *Powder Technol.*, vol. 337, pp. 111–118, Sep. 2018.

[16] S. Morrell and I. Stephenson, "Slurry discharge capacity of autogenous and semi-autogenous mills and the effect of grate design," *Int. J. Mineral Process.*, vol. 46, nos. 1–2, pp. 53–72, Apr. 1996.

[17] S. Morrell, "Modelling the influence on power draw of the slurry phase in autogenous (AG), semi-autogenous (SAG) and ball mills," *Minerals Eng.*, vol. 89, pp. 148–156, Apr. 2016.

[18] S. Latchireddi and S. Morrell, "Slurry flow in mills: Grate-only discharge mechanism (Part-1)," *Minerals Eng.*, vol. 16, no. 7, pp. 625–633, Jul. 2003.

[19] S. Latchireddi and S. Morrell, "Slurry flow in mills: Grate-pulp lifter discharge systems (Part 2)," *Minerals Eng.*, vol. 16, no. 7, pp. 635–642, Jul. 2003.

[20] Y.-D. Ko and H. Shang, "Time delay neural network modeling for particle size in SAG mills," *Powder Technol.*, vol. 205, nos. 1–3, pp. 250–262, Jan. 2011.

[21] P. Pourghahramani, "Effects of ore characteristics on product shape properties and breakage mechanisms in industrial SAG mills," *Minerals Eng.*, vol. 32, pp. 30–37, May 2012.

[22] F. Núñez, D. Silva, and A. Cipriano, "Characterization and modeling of semi-autogenous mill performance under ore size distribution disturbances," *IFAC Proc. Volumes*, vol. 44, no. 1, pp. 9941–9946, Jan. 2011.

[23] F. A. Lucay, E. D. Gálvez, M. Salez-Cruz, and L. A. Cisternas, "Improving milling operation using uncertainty and global sensitivity analyses," *Minerals Eng.*, vol. 131, pp. 249–261, Jan. 2019.

CHENG YUWEN received the B.E. degree in electrical engineering from Yanshan University, Qinhuangdao, China, in 2018. He is currently pursuing the master's degree with the School of Control Science and Engineering, Shandong University, Jinan, China. His research interests include modeling, parameter estimation, and integrated automation of complex industrial processes.

BO SUN received the B.S. and Ph.D. degrees from Shandong University, China, in 2004 and 2009, respectively.

In 2010, he joined Shandong University, where he is currently an Associate Professor with the School of Control Science and Engineering. His current research interests include the optimal control of engineering and the optimization of combined cooling, heating, and power systems.

SHUAI LIU received the B.E. and M.E. degrees in control theory and engineering from Shandong University, China, in 2004 and 2007, respectively, and the Ph.D. degree in electrical and electronic engineering from Nanyang Technological University, Singapore, in 2012. He was a Senior Research Fellow with Berkeley Education Alliance for Research in Singapore (BEARS), from 2011 to 2017. Since 2017, he has been with the School of Control Science and Engineering, Shandong University. His research interests include modeling, cooperative control, distributed consensus, optimal estimation and control, time-delay systems, fault detection, and estimation.

● ● ●